

Numerical simulations of an incompressible piezoviscous fluid flowing in a plane slider bearing*

Martin Lanzendörfer

Josef Málek

Kumbakonam R. Rajagopal[†]

Abstract

We provide numerical simulations of an incompressible pressure-thickening and shear-thinning lubricant flowing in a plane slider bearing. We study the influence of several parameters, namely the ratio of the characteristic lengths $\varepsilon > 0$ (with $\varepsilon \searrow 0$ representing the Reynolds lubrication approximation); the coefficient of the exponential pressure–viscosity relation $\alpha^* \geq 0$; the parameter $G^* \geq 0$ related to the Carreau–Yasuda shear-thinning model and the modified Reynolds number $\text{Re}_\varepsilon \geq 0$. The finite element approximations to the steady isothermal flows are computed without resorting to the lubrication approximation. We obtain the numerical solutions as long as the variation of the viscous stress $\mathbf{S} = 2\eta(p, \text{tr}\mathbf{D}^2)\mathbf{D}$ with the pressure is limited, say $|\partial\mathbf{S}/\partial p| \leq 1$. We show conclusively that the existing practice of avoiding the numerical difficulties by cutting the viscosity off for large pressures leads to results that depend solely on the artificial cut-off parameter. We observe that the piezoviscous rheology generates pressure differences across the fluid film.

1 Introduction

Lubrication problems represent a set of important engineering applications that have been a source of inspiration for a great deal of research in fluid dynamics. The plane slider flow described in the next section embodies a classical prototype of hydrodynamic lubrication. Two solid surfaces in relative motion are separated by a thin layer of a liquid lubricant, the fluid film being thick enough still to separate the surfaces completely. Since the fundamental work by Reynolds [38], the *lubrication approximation* approach, which considerably reduces the system of equations governing the thin film flow, proved to be a very useful and flexible tool.

Within the class of lubrication problems, one that presents challenging issues is Elastohydrodynamic Lubrication (EHL) wherein one encounters extremely high peak pressures¹ of

the order of a GPa, very high shear rates, significant variations in temperature (see [4, 5]), and deformation of the solid boundary (see [40]). The competing effects of the increase of the viscosity due to the high pressures, and the decrease of the viscosity due to the shear thinning at high shear rates as well as increases in temperature present further challenges both with regard to rigorous mathematical and numerical analysis, and computation.

Alongside the Reynolds approximation approach, which has served as the exclusive tool for engineering predictions, the more general tools of Computational Fluid Dynamics (CFD) were brought to bear on lubrication problems recently, e.g. [1–3, 9, 20, 26]. CFD simulations are expected to allow one to get a more detailed and accurate understanding of the flow involved in the lubrication problems, that cannot be achieved within the context of the Reynolds approximation, especially with regard to problems involving starved lubrication, problems involving rough and dimpled surfaces, cavitation, or more complex rheology or geometry, see [31] for relevant references. It is worth noting that the available numerical results based on solving the full system of equations governing the flow have not considered the heavily loaded regimes so far.

The present paper focuses on a particular issue pointed out already by Bair et al. [6], that the pressure-thickening response itself eventually causes the violation of the lubrication assumptions. Namely, that a gradient of pressure in the direction across the film is generated in the flow. The same observation has led to the revision of Reynolds equation in the piezoviscous regime, see [7, 18, 36]. Yet another important consequence of this rather specific feature of piezoviscous fluids is that the momentum equation describing the flow exhibits structural changes, once certain threshold of the pressure and shear rate is reached. This is well reflected in the results that are available concerning the existence and uniqueness of weak solutions, which are based on assumptions that allow for the realistic pressure- and shear rate- viscosity relations only up to that threshold, see the references in Sect. 3.

Bearing this in mind, in contrast to the previous studies based on the CFD approach referred above, we restrict ourselves to a simpler setting. This allows us to focus on some important issues, which we believe are characteristic of more realistic models as well but which have not been studied in the detail that they deserve in the literature so far.

non-Newtonian fluids (see [35] for a detailed discussion of the concept of “pressure”). In this study, “pressure” signifies the mean normal stress.

*Submitted to Meccanica on January 11, 2017. The final publication is available at Springer via <http://dx.doi.org/10.1007/s11012-017-0731-0>.

[†]M. Lanzendörfer, J. Málek, Mathematical Institute, Faculty of Mathematics and Physics, Charles University, Prague, Czech Republic. J. Málek acknowledges the support of the ERC-CZ project LL1202 financed by MŠMT (Ministry of Education, Youth and Sports of the Czech Republic). K. R. Rajagopal, Department of Mechanical Engineering, Texas A&M University, United States. K. R. Rajagopal thanks the National Science Foundation, United States for its support.

¹ The terminology “pressure” has been used to define a variety of disparate quantities and can be a source for a great deal of confusion, especially when discussing lubricants since many lubricants that are used are

In Sect. 2 we recall the partial differential equations governing the planar steady isothermal flow of a homogeneous incompressible viscous fluid and we develop the dimensionless governing equations within the context of the plane slider geometry. The boundary conditions for the inflow and outflow boundaries of the domain are discussed in Sect. 2.3 in detail. We describe the pressure-thickening and shear-thinning rheology provided by the Carreau–Yasuda relation with the exponential pressure–viscosity law. Such rheology is simple enough for the purpose of discussing how the dimensionless parameters affect the flow. At the same time, it provides a realistic model that is not altered to fit into any class of constitutive relations accessible by the theoretical existence and uniqueness results available.

In Sect. 3 we introduce the finite element approximations to be used for carrying out the numerical simulations. We recall the current limitations of both the theoretical well-posedness results available and of the numerical approach based on the Galerkin (finite element) approximations. We discuss the constraint with regard to the variation of the viscous stress with the pressure, which is observed in numerical experiments and is analogous to the assumptions needed to establish existence results in the theoretical works. We are able to carry out the numerical simulations only within a certain range of pressure and shear rate where the constraint is met.

Sect. 4 starts by demonstrating the basic features of the flow in the case of Navier–Stokes fluid. Then we incorporate the pressure–viscosity relation into the problem and carry out a set of numerical simulations with $\eta = \eta_0 e^{\alpha p}$, $\alpha > 0$. It is customary in numerical computations to avoid numerical difficulties by cutting the viscosity off above given threshold for the pressure. We document by numerical calculations in Sect. 4.2, that such a procedure may actually lead to very different results for the problem under consideration, depending on the cut-off parameter. Therefore, there is no cut-off utilised in the subsequent results presented in Sect. 4. We show that the response of a piezoviscous fluid leads to variations of pressure across the film in Sect. 4.3. Finally, we study the consequences of the fluid being shear-thinning and we also determine the effect of inertia on the characteristics of the flow.

2 Setting of the mathematical problem

2.1 Governing equations

We consider a planar steady isothermal flow of a homogeneous incompressible viscous fluid, governed by the system of equations

$$(1) \quad \left. \begin{aligned} \operatorname{div} \mathbf{v} &= 0 \\ \operatorname{div}(\rho \mathbf{v} \otimes \mathbf{v}) - \operatorname{div} \mathbf{T} &= \mathbf{f} \end{aligned} \right\} \text{ in } \Omega \subset \mathbb{R}^2,$$

where the Cauchy stress tensor \mathbf{T} is given by the relation

$$(2) \quad \mathbf{T} = -p\mathbf{I} + 2\eta(p, \operatorname{tr} \mathbf{D}^2) \mathbf{D}.$$

The unknowns are the velocity \mathbf{v} and the pressure p , while the given data are the density ρ , the body force \mathbf{f} and the relation $\eta = \eta(p, \operatorname{tr} \mathbf{D}^2)$, which characterizes the viscosity of a pressure-thickening and shear-thinning lubricant. In the above equation $\mathbf{D} = \frac{1}{2}(\nabla \mathbf{v} + (\nabla \mathbf{v})^T)$ denotes the symmetric part of the velocity gradient. Note that here p coincides with the mean value stress $m = -\frac{1}{2} \operatorname{tr} \mathbf{T}$, by virtue of $\operatorname{tr} \mathbf{D} = \operatorname{div} \mathbf{v} = 0$, cf. [34].

The assumption of the flow being isothermal is made for the sake of simplicity. Similarly, we do not allow for elastic deformation of the solid surfaces, so that a flow in the fixed domain Ω is considered instead. Note also that we implicitly assume that the resulting pressure field would remain positive throughout the domain, so that we need not discuss the possibility of cavitation within the flow. Since we study the flow in between converging surfaces, the latter assumption is reasonable.

2.2 Plane slider geometry

The geometry of the plane slider is illustrated in Fig. 1a. The rigid slider is fixed in the space above the horizontal plane which is moving in the horizontal direction steadily with the speed U . The lubricating fluid is dragged by the moving plane and forced through the converging gap. The two solid surfaces define the natural boundaries Γ_{plane} , Γ_{slider} of the domain Ω , while the two artificial boundaries Γ_{in} , Γ_{out} are defined at the inlet and outlet. The length of the domain is usually denoted by B , and h_1 , h_2 denote the height of the fluid film at the outlet and inlet, respectively.

A crucial feature of the lubrication problem is that $h = \frac{1}{2}(h_1 + h_2)$ is much smaller than B , that is

$$h = \varepsilon B, \quad \text{where } \varepsilon \ll 1.$$

We exploit this feature in the dimensionless formulation of the governing equations in Sect. 2.4. Note that apart from B , the geometry of the plane slider is characterized by two dimensionless parameters, ε and the ratio h_2/h_1 .

2.3 Boundary conditions

We assume no-slip conditions at the solid walls, i.e., that the velocity of the fluid vanishes on the upper surface, while on the lower plate it equals the given tangential velocity

$$(3) \quad \mathbf{v} = \mathbf{0} \text{ on } \Gamma_{\text{slider}} \quad \text{and} \quad \mathbf{v} = (-U, 0) \text{ on } \Gamma_{\text{plane}}, \quad U > 0.$$

The inflow and outflow boundaries are artificial, subject to a mass flux that is not known a priori. Therefore, there is no obvious proper choice for boundary conditions on Γ_{in} and Γ_{out} . A detailed discussion of different possibilities is out of the scope of the present study. For the moment, let us merely refer the reader to [21], appending the following remarks related to the particular situation in the plane slider.

When using the Reynolds approximation, one arrives at a single equation for the pressure, the velocity being dealt

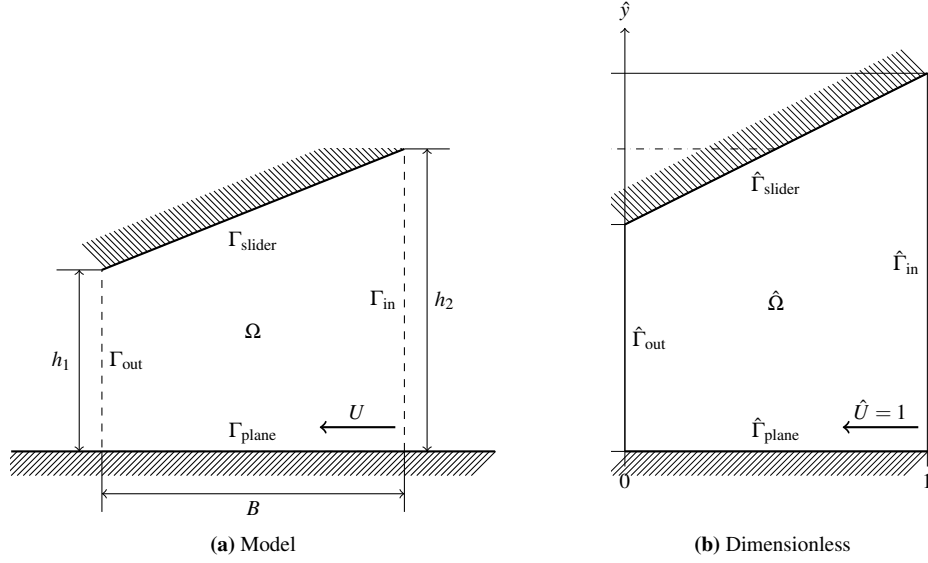


Figure 1: Plane slider geometry

with implicitly within the context of lubrication assumptions. It is then straightforward to prescribe

$$(4) \quad p = P_0 \in \mathbb{R} \quad \text{at both the inlet and outlet,}$$

where, most often, $P_0 = 0$ is chosen to represent the ambient pressure (since that is presumably negligible compared to the pressure generated within the flow). It is worth mentioning that for higher values of Re_e (the modified Reynolds number as defined in Sect. 2.4) the inlet and outlet conditions for the Reynolds approximation should include the influence of the fluid inertia as well, see e.g. [10].

In contrast, when the weak solution to (1) is considered, the quantities naturally defined on the boundary are the vectors of velocity \mathbf{v} and traction $-\mathbf{T}\mathbf{n}$ (\mathbf{n} denotes the outer normal vector). Surprisingly, the boundary conditions on artificial boundaries seem to be an issue that has not yet been unequivocally resolved in the literature. Moreover, we should bear in mind two particular aspects of this study, namely: (a) that it should be possible to relate the problem setting to the Reynolds approximation approach, and (b) that we are keen to relate the variations of the pressure across the film to the piezoviscous response of the fluid. To this end, we take advantage of the boundary condition which (a) results in the pressure values being equal or approximately equal to the given constant P_0 and (b) does not induce cross flow and pressure variations in the vicinity of the artificial boundary.

Therefore, we prescribe

$$(5) \quad \begin{aligned} &-\mathbf{T}\mathbf{n} = \mathbf{b}_n + \mathbf{b}_\tau \quad \text{on } \Gamma_{\text{in}} \cup \Gamma_{\text{out}}, \\ &\text{where } \mathbf{b}_n = P_0 \mathbf{n} \quad \text{and } \mathbf{b}_\tau = \eta (\nabla \mathbf{v} - (\nabla \mathbf{v})^T) \mathbf{n}. \end{aligned}$$

Note that $\mathbf{b}_\tau \cdot \mathbf{n} = 0$. Denoting $[\mathbf{w}]_\tau \stackrel{\text{def}}{=} \mathbf{w} - (\mathbf{w} \cdot \mathbf{n}) \mathbf{n}$, one notices that $[\mathbf{b}_n]_\tau = 0$. The notation \mathbf{b}_n and \mathbf{b}_τ thus corresponds to the decomposition of the prescribed traction into its normal and tangential parts. We make the following observations concerning the above two terms.

First, the available theoretical results that guarantee the existence (and for small data, in certain sense, the uniqueness) of the weak solution to the system (1) require, as one of the assumptions, that

$$(6) \quad \begin{aligned} &-\mathbf{T}\mathbf{n} = \mathbf{b}(\mathbf{v}) \quad \text{on } \Gamma_{\text{in}} \cup \Gamma_{\text{out}}, \\ &\text{where } \mathbf{b}(\mathbf{v}) \cdot \mathbf{v} \geq -\frac{\rho}{2} |\mathbf{v}|^2 (\mathbf{v} \cdot \mathbf{n}) + C \end{aligned}$$

is prescribed, where C represents terms supposed to be of lower order in \mathbf{v} . If (6) is not ensured then one cannot derive the standard energy estimates, and a weak solution with bounded kinetic energy is not necessarily found. In the case of constant viscosity (i.e., for steady Navier–Stokes equations) this is well known, see e.g. [8, 27, 33]; the case of viscosity depending on pressure and shear rate is not different in this particular regard, see [29]. Note in particular, that (6) does not allow one to prescribe the normal component of the traction independent of the velocity. Neither (5), nor the condition prescribing the constant traction,

$$(7) \quad -\mathbf{T}\mathbf{n} = P_0 \mathbf{n},$$

nor, e.g., the boundary condition

$$(8) \quad p\mathbf{n} - \eta \frac{\partial \mathbf{v}}{\partial \mathbf{n}} = P_0 \mathbf{n},$$

are covered by (6). The latter is well known as the *do-nothing* condition in the case that the viscosity is constant and that $P_0 = 0$. In fact, in the case of a radial flow, one can observe both the trivial and a non-trivial solution for trivial boundary data, using any of the boundary conditions² (5), (7) or (8). Even in the case of flow in straight channels or, importantly,

² To present such examples in detail would be out of the scope of this study and is a subject of a work in preparation by J. Hron and M. Lanzendörfer.

the plane slider flow, one may indeed encounter complications in finding the numerical solution (observing a numerical blow-up of the kinetic energy in the approximate solution iterates). However, such difficulties were not observed within the range of parameters presented in this paper.

Note that in case of pure outflow, $\mathbf{v} \cdot \mathbf{n} \geq 0$, the term that is cubic in the velocity in (6) is negative and does not represent a restriction on \mathbf{b} . This is why (6) does not restrain one to use (7) or (8) in practical computations for outflow boundary conditions, as long as no backward flow is expected. At the inflow, the velocity profile is then usually given explicitly as

$$\mathbf{v} = \mathbf{v}_{\text{in}}.$$

We remark that the above specification is not suitable for the plane slider problem and for most lubrication problems, since \mathbf{v}_{in} would not be known a priori (not even the flux $\int_{\Gamma_{\text{in}}} \mathbf{v} \cdot \mathbf{n} \, ds$).

Note also that based on (6) one could arrive at the idea of prescribing, e.g.,

$$\mathbf{b}_n(\mathbf{v}) = \left(P_0 - \frac{\rho}{2} |\mathbf{v}|^2 \right) \mathbf{n}.$$

Such a choice would lead to significant variations of the normal traction $-\mathbf{T}\mathbf{n} \cdot \mathbf{n}$ (and, consequently, of the resulting pressure) across the film and to a concomitant cross-flow in the vicinity of both artificial boundaries, even in the case of the flow between parallel plates. In contrast, (5) gives the normal traction $-\mathbf{T}\mathbf{n} \cdot \mathbf{n} = \mathbf{b}_n \cdot \mathbf{n} = P_0$ which is constant across the film and is satisfied by simple unidirectional flows.

Second, the particular relation for \mathbf{b}_τ in (5) was also chosen for the purpose of avoiding the pressure variations along the artificial boundary. Indeed, the condition $\mathbf{b}_\tau = \mathbf{0}$ (7) is not satisfied by simple unidirectional flows and it would result in the flow with the streamlines distorted and with the sharp pressure artifacts near the corners adjacent to the artificial boundary, see the discussion and numerical examples in [21]. In contrast, with \mathbf{b}_τ from (5) one can infer (formally, i.e. assuming that all the quantities are well defined on the boundary) that

$$\begin{aligned} \mathbf{0} = [\mathbf{T}\mathbf{n} + \mathbf{b}_\tau]_\tau &= [-p\mathbf{n} + \eta(\nabla\mathbf{v} + (\nabla\mathbf{v})^T)\mathbf{n} \\ &\quad + \eta(\nabla\mathbf{v} - (\nabla\mathbf{v})^T)\mathbf{n}]_\tau = 2\eta[(\nabla\mathbf{v})\mathbf{n}]_\tau \end{aligned}$$

implying, due to the viscosity being positive (while it need not be a constant), that

$$\left[\frac{\partial\mathbf{v}}{\partial\mathbf{n}} \right]_\tau = \frac{\partial[\mathbf{v}]_\tau}{\partial\mathbf{n}} = \mathbf{0}.$$

This relation seems to have no physical interpretation except that, notably, it is satisfied by unidirectional flows perpendicular to the artificial boundary (i.e., when $[\mathbf{v}]_\tau \equiv \mathbf{0}$). In other words, (5) does not induce cross-flow at the vicinity of inflow and outflow boundaries, allowing thus for straight streamlines and the pressure field with no local artifacts in the corners.

Note that (5) can be formally rewritten as

$$p\mathbf{n} - 2\eta \frac{\partial\mathbf{v}}{\partial\mathbf{n}} = P_0\mathbf{n},$$

a form similar to (8). For Navier–Stokes equations, due to the constraint of incompressibility $\text{div}\mathbf{v} = 0$ and due to the viscosity being constant, the following $\text{div}\mathbf{T} = \text{div}(-p\mathbf{I} + \eta(\nabla\mathbf{v}))$ holds. If the weak formulation is based on this form involving the full velocity gradient, then the *do-nothing* boundary condition (8) with $P_0 = 0$ corresponds to the trivial (zero) boundary term in the weak formulation, see [21] for details. For fluids with variable viscosity, however, to define the weak solution based on the Cauchy stress tensor \mathbf{T} and to give the boundary data in terms of the traction $-\mathbf{T}\mathbf{n}$ is more appropriate. In this sense and in view of the previous paragraph, one can look on (5) as a generalization of the *do-nothing* boundary condition in the case of variable viscosity.

To our knowledge, there is no result concerning the existence of weak solutions to (1) that would cover the presence of \mathbf{b}_τ defined in (5) in the boundary data. The available theory is built upon uniform estimates for \mathbf{v} in the Sobolev space $\mathbf{W}^{1,r}(\Omega)$, $1 < r \leq 2$, and does not allow one to treat the gradients of velocity on the boundary. Nevertheless, we did not encounter any complications related to \mathbf{b}_τ in our numerical computations.

2.4 The dimensionless formulation of (1)

Let us rewrite the governing equations using the dimensionless variables (indicated by hat). Denote $\mathbf{x} = (x, y)$, $\mathbf{v} = (u, v)$ and $\hat{\mathbf{x}}$, $\hat{\mathbf{v}}$ analogously. For simplicity, we neglect the body forces by assuming that $\mathbf{f} = \mathbf{0}$ and make use of that the fluid is homogeneous and incompressible by taking $\rho = \rho^* \equiv \text{const}$. We define

$$\begin{aligned} x &= X^* \hat{x}, & u &= U^* \hat{u}, & p &= P^* \hat{p}, & \eta &= \eta^* \hat{\eta}, \\ y &= \varepsilon X^* \hat{y}, & v &= \varepsilon U^* \hat{v}, \end{aligned}$$

For the plane slider problem, we take $X^* = B$ and $U^* = U$ for the characteristic length and velocity. As illustrated in Fig. 1b, the plane slider geometry Ω transforms into the dimensionless $\hat{\Omega} = \{(\hat{x}, \hat{y}) : \hat{x} \in (0, 1), \hat{y} \in (0, \hat{h}(\hat{x}))\}$, where $\hat{h}(\hat{x}) = \hat{h}_1 + \hat{x}(\hat{h}_2 - \hat{h}_1)$ and $\hat{h}_1 = \frac{2}{1+(h_2/h_1)}$, $\hat{h}_2 = \frac{2(h_2/h_1)}{1+(h_2/h_1)}$. For more details see, e.g., [40].

We set η^* to be the viscosity at negligible shear rates and pressure and define the characteristic pressure P^* and the modified Reynolds number Re_ε (leaving Re for the standard Reynolds number) as customary by

$$P^* = \frac{\eta^* U^*}{\varepsilon^2 X^*} \quad \text{and} \quad \text{Re}_\varepsilon = \varepsilon \text{Re} = \frac{\varepsilon^2 \rho^* X^* U^*}{\eta^*} = \frac{\rho^* U^{*2}}{P^*}.$$

Setting $\text{Re}_\varepsilon = 0$ represents Stokes-type flow, where the inertia of the fluid is neglected. One easily rewrites (1) as

$$(9) \quad \left. \begin{aligned} \text{div}_{\hat{\mathbf{x}}} \hat{\mathbf{v}} &= 0 \\ \text{Re}_\varepsilon \left(\begin{array}{l} \hat{\mathbf{v}} \cdot \nabla_{\hat{\mathbf{x}}} u \\ \varepsilon^2 \hat{\mathbf{v}} \cdot \nabla_{\hat{\mathbf{x}}} v \end{array} \right) - \text{div}_{\hat{\mathbf{x}}} \tilde{\mathbf{T}} &= \mathbf{0} \end{aligned} \right\} \text{ in } \hat{\Omega},$$

where $\tilde{\mathbf{T}} = -\hat{p}\mathbf{I} + 2\hat{\eta}\tilde{\mathbf{D}}_\varepsilon$ and

$$(10) \quad \tilde{\mathbf{D}}_\varepsilon = \frac{1}{2} \begin{pmatrix} 2\varepsilon^2\partial_{\hat{x}}\hat{u} & \varepsilon^2\partial_{\hat{x}}\hat{v} + \partial_{\hat{y}}\hat{u} \\ \varepsilon^4\partial_{\hat{x}}\hat{v} + \varepsilon^2\partial_{\hat{y}}\hat{u} & 2\varepsilon^2\partial_{\hat{y}}\hat{v} \end{pmatrix}.$$

Note that $\tilde{\mathbf{T}}$ differs from $\hat{\mathbf{T}}$ defined by $\mathbf{T} = P^*\hat{\mathbf{T}}$, wherein $\hat{\mathbf{T}} = -\hat{p}\mathbf{I} + 2\hat{\eta}\varepsilon\hat{\mathbf{D}}_\varepsilon$ and

$$(11) \quad \hat{\mathbf{D}}_\varepsilon = \frac{1}{2} \begin{pmatrix} 2\varepsilon\partial_{\hat{x}}\hat{u} & \varepsilon^2\partial_{\hat{x}}\hat{v} + \partial_{\hat{y}}\hat{u} \\ \varepsilon^2\partial_{\hat{x}}\hat{v} + \partial_{\hat{y}}\hat{u} & 2\varepsilon\partial_{\hat{y}}\hat{v} \end{pmatrix}.$$

The no-slip boundary condition (3) takes the simple form

$$(12) \quad \hat{\mathbf{v}} = \mathbf{0} \text{ on } \hat{\Gamma}_{\text{slider}} \quad \text{and} \quad \hat{\mathbf{v}} = (-1, 0) \text{ on } \hat{\Gamma}_{\text{plane}}.$$

Following (10), one can easily derive (here we take the advantage of that the artificial boundary is perpendicular to the x -axis, so that $\mathbf{n} = \pm(1, 0) = \hat{\mathbf{n}}$ holds) that (5) takes the dimensionless form

$$(13) \quad -\tilde{\mathbf{T}}\hat{\mathbf{n}} = \hat{\mathbf{b}} \stackrel{\text{def}}{=} \begin{cases} (\hat{P}_0, \hat{b}_\tau) & \text{on } \hat{\Gamma}_{\text{in}}, \\ -(\hat{P}_0, \hat{b}_\tau) & \text{on } \hat{\Gamma}_{\text{out}}, \end{cases}$$

where $\hat{P}_0 = P_0/P^*$ and $\hat{b}_\tau = \hat{\eta}(\varepsilon^4\partial_{\hat{x}}\hat{v} - \varepsilon^2\partial_{\hat{y}}\hat{u})$. Note in particular, that (5) reduces formally to (4) when the lubrication assumptions are taken, namely when $\partial[\mathbf{v}]_\tau/\partial\mathbf{n}$ and $\partial(\mathbf{v}\cdot\mathbf{n})/\partial\mathbf{n}$ can be neglected.

2.5 Viscosity

We are interested in lubrication problems wherein the range of pressures involved is very large and in virtue of which the viscosity of the fluid changes by several orders of magnitude, in fact by as much as 10^6 or 10^8 . That this is indeed the case is borne out by experiments. It is also well known that many lubricants shear-thin and thus we employ the model wherein the viscosity depends on both the pressure and the shear rate (in the general three dimensional or planar flow on the norm of the symmetric part of the velocity gradient). Several correlations have been used to describe the variation of the viscosity with pressure. In this study we will follow the model suggested by Bair [4] where the viscosity is related to the pressure and to the Frobenius norm of the velocity gradient through the Carreau–Yasuda relationship. We shall specifically assume that the viscosity is given by the following relation, with $\eta_0 > 0$, $1 < r < 2$,

$$(14) \quad \eta = \eta_0 a(p) (1 + b(p) \text{tr}\mathbf{D}^2)^{\frac{r-2}{2}},$$

where $a(\cdot)$, $b(\cdot)$ are given functions³ of the pressure p . In order to simplify the discussion of the numerical results in the

³ The three reference lubricants presented by Bair [4] are characterized as compressible, their viscous response depending on the density and temperature,

$$\eta \equiv \eta_{\text{com}}(\rho, \text{tr}\mathbf{D}^2, \vartheta).$$

In view of incompressibility and the assumption of isothermal conditions, we consider the pressure and shear-rate dependent viscosity only, i.e.

$$\eta \stackrel{\text{def}}{=} \eta(p, \text{tr}\mathbf{D}^2) = \eta_{\text{com}}(\rho_{\text{com}}(p, \vartheta), \text{tr}\mathbf{D}^2, \vartheta),$$

where the material properties are considered at constant temperature and where the density $\rho_{\text{com}}(p, \vartheta)$ merely provides the correct dependence of the viscosity on the pressure, the actual density considered in the momentum conservation being constant.

dimensionless formulation of the problem, we take the idealized exponential model for the pressure–viscosity dependence $a(p)$ and an analogous simple relation for the shifting rule $b(p)$, i.e., with $\eta_0, G, \alpha, \beta > 0$, $1 < r < 2$,

$$(15) \quad \eta = \eta_0 e^{\alpha p} \left(1 + G e^{\beta p} \text{tr}\mathbf{D}^2\right)^{\frac{r-2}{2}}.$$

Note that for small shear rates, (15) reduces to

$$\eta \sim \eta_0 e^{\alpha p} \quad (\text{for } \text{tr}\mathbf{D}^2 \ll e^{-\beta p}/G),$$

while for large shear rates there is, with $\tilde{\beta} = \alpha - \frac{2-r}{2}\beta$,

$$\eta \sim \eta_0 e^{\tilde{\beta} p} \sqrt{G \text{tr}\mathbf{D}^2}^{r-2} \quad (\text{for } \text{tr}\mathbf{D}^2 \gg e^{-\beta p}/G).$$

Finally, it follows from the definition of $\hat{\mathbf{D}}_\varepsilon$ from (11) that⁴

$$\text{tr}\mathbf{D}^2 = D^{*2} \text{tr}\hat{\mathbf{D}}_\varepsilon^2, \quad \text{where } D^* = \frac{U^*}{\varepsilon X^*},$$

whereby we obtain the following dimensionless form of (15),

$$(16) \quad \hat{\eta} = e^{\alpha^* \hat{p}} \left(1 + G^* e^{\beta^* \hat{p}} \text{tr}\hat{\mathbf{D}}_\varepsilon^2\right)^{\frac{r-2}{2}},$$

provided that

$$\alpha^* = \alpha P^*, \quad \beta^* = \beta P^*, \quad G^* = G D^{*2} \quad \text{and} \quad \eta^* = \eta_0.$$

The numerical simulations presented in what follows will be restricted, for the sake of simplicity, to $r = 3/2$ and $\beta/\alpha = \beta^*/\alpha^* = 2$, leaving two remaining parameters: α^* and G^* .

3 Numerical solution

We approximate the problem described by (9), (10), (12), (13) and (16) using the following Galerkin formulation: Find $(\hat{\mathbf{v}}_l, \hat{p}_l) \in (\hat{\mathbf{v}}_0 + \mathbf{X}_l) \times \mathcal{Q}_l$ (the discrete solution) such that

$$(17) \quad \int_{\hat{\Omega}} (\text{div}_{\hat{\mathbf{x}}}\hat{\mathbf{v}}_l) q \, d\hat{x} = 0 \quad \forall q \in \mathcal{Q}_l,$$

$$(18) \quad \text{Re}_\varepsilon \int_{\hat{\Omega}} \begin{pmatrix} \hat{\mathbf{v}}_l \cdot \nabla_{\hat{\mathbf{x}}} u_l \\ \varepsilon^2 \hat{\mathbf{v}}_l \cdot \nabla_{\hat{\mathbf{x}}} v_l \end{pmatrix} \cdot \mathbf{w} \, d\hat{x} + \int_{\hat{\Omega}} \tilde{\mathbf{T}}_l \cdot \nabla_{\hat{\mathbf{x}}} \mathbf{w} \, d\hat{x} \\ + \int_{\hat{\Gamma}_{\text{in}} \cup \hat{\Gamma}_{\text{out}}} \hat{\mathbf{b}}_l \cdot \mathbf{w} \, d\hat{s} = 0 \quad \forall \mathbf{w} \in \mathbf{X}_l,$$

with $\tilde{\mathbf{T}}_l, \hat{\mathbf{b}}_l$ given by (10), (13) and (16). The parameter $l > 0$ is related to the finite-dimensional function spaces $\mathcal{Q}_l, \mathbf{X}_l$,

$$\mathcal{Q}_l \subset L^1(\hat{\Omega}) \quad \text{and}$$

$$\mathbf{X}_l \subset \{\mathbf{w} \in W^{1,1}(\hat{\Omega})^2; \mathbf{w} = \mathbf{0} \text{ on } \hat{\Gamma}_{\text{slider}} \cup \hat{\Gamma}_{\text{plane}}\}$$

and $\hat{\mathbf{v}}_0$ is a suitable extension of the Dirichlet data (12). Naturally, $\mathbf{X}_l, \mathcal{Q}_l$ are to be chosen such that all the integrals are well defined and finite.

⁴Note that D^* represents the characteristic shear rate. Note also that $\text{tr}\hat{\mathbf{D}}_\varepsilon^2 \sim \frac{1}{2}(\partial_{\hat{y}}\hat{u})^2$, as $\varepsilon \searrow 0$.

The numerical simulations presented in this work are based on the following finite element approach. The domain $\hat{\Omega}$ is discretized by means of quadrilaterals (of diameter l at most) and \mathbf{X}_l , \mathcal{Q}_l are generated by the second order $\mathbb{Q}_2/\mathbb{P}_{-1}$ finite element pair described in [17, 39] (the conforming bi-quadratic elements for the velocity and the discontinuous piecewise linear space for the pressure). The resulting system of nonlinear algebraic equations is solved using the damped Newton method with line search, with the Jacobian matrix approximated by the central differences. The linear subproblems, sparse and unsymmetric, are mostly solved by the direct sparse LU factorization implemented in the UMFPAK package, see [15]. The presented numerical simulations are performed on a regular mesh of $3 \cdot 4^6$ finite elements, corresponding 136 194 degrees of freedom.

In an ideal situation, letting the discretization parameter $l \searrow 0$ and hence the dimension of the finite element function spaces \mathbf{X}_l , \mathcal{Q}_l to infinity, the error due to discretization would vanish and the discrete solution (\mathbf{v}_l, p_l) would eventually converge to a (weak) solution (\mathbf{v}, p) . This desired behaviour has been guaranteed rigorously in [22] after making additional requirements which, however, do not cover realistic viscosity (15) at large pressures. The result in [22] stems from intensive research devoted to the notion and existence of a weak solution for incompressible fluids with pressure- and shear rate- dependent viscosity, see [11, 12, 16, 28] (see also [13, 24, 25, 37] and the references therein). One of the assumptions embodied in the theoretical framework requires in particular that

$$(19) \quad \left\| \frac{\partial \mathbf{S}}{\partial p} \right\| \leq C \leq 1, \quad \text{where } \mathbf{S} = \mathbf{T} + p\mathbf{I} = 2\eta\mathbf{D},$$

for certain constant C , see the concerned results for details⁵.

⁵One of the key steps when proving the existence of a weak solution, to put it in a simple way, is to establish the uniqueness of the pressure field p provided that the velocity field of the solution \mathbf{u} is given. Depending on the setting of the problem (which includes a number of assumptions concerning the domain geometry, the boundary conditions given, the parameters of the rheology, etc.) one should be able to obtain the inequality of the following type

$$0 < C < \inf_{q \in \mathcal{Q}} \sup_{\boldsymbol{\psi} \in \mathbf{X}} \frac{\int_{\Omega} q \operatorname{div} \boldsymbol{\psi} \, dx}{\|q\|_2 \|\nabla \boldsymbol{\psi}\|_2},$$

where the functional spaces (and the corresponding norms in the above inequality) for the pressure and velocity, \mathcal{Q} and \mathbf{X} , and the constant $0 < C \leq 1$ would depend on the particular setting. Here let us say $\mathcal{Q} \subset L^2(\Omega)$ and $\mathbf{X} \subset \{\boldsymbol{\psi}; \nabla \boldsymbol{\psi} \in L^2(\Omega)\}$.

With help of the above inequality and using the weak momentum equation, one can estimate for two pressure fields p_1 , p_2 and the given velocity field \mathbf{u} that the following

$$\begin{aligned} C\|p_1 - p_2\|_2 &\leq \sup_{\|\nabla \boldsymbol{\psi}\|_2=1} \int_{\Omega} (p_1 - p_2) \operatorname{div} \boldsymbol{\psi} \, dx \\ &= \sup_{\|\nabla \boldsymbol{\psi}\|_2=1} \int_{\Omega} (\mathbf{S}(p_1, \mathbf{D}) - \mathbf{S}(p_2, \mathbf{D})) \cdot \nabla \boldsymbol{\psi} \, dx \end{aligned}$$

holds. One obtains the result by estimating the last term by

$$\begin{aligned} \dots &\leq \|\mathbf{S}(p_1, \mathbf{D}) - \mathbf{S}(p_2, \mathbf{D})\|_2 \\ &\leq \left\| |p_1 - p_2| \int_{p_1}^{p_2} \frac{\partial \mathbf{S}(p_1 + s(p_2 - p_1), \mathbf{D})}{\partial p} \, ds \right\|_2 < C\|p_1 - p_2\|_2, \end{aligned}$$

provided that $|\partial \mathbf{S} / \partial p| < C$.

Note that (15) with $\alpha > 0$ violates (19) *both* at elevated pressures *or* high shear rates. For (15), the notion of a solution such that the problem would be well posed remain a challenging open problem, as far as no a priori restrictions on the data size are imposed.

On the basis of our numerical computations, including those presented in the next section, (19) seems to be both sufficient and necessary (with $C = 1$, or nearly so) for the presented numerical approach to converge successfully. Once (19) is violated by the approximate solution at hand, we were unable to obtain any discrete solution. An analogous restriction seems to apply for previously published results in a more complex setting as well, cf. [1, 26].

For the sake of completeness we recall that there are no theoretical well-posedness results allowing for the boundary condition (5), as discussed already in Sect. 2.3, cf. [29]. Note also that some lower values of the parameter $1 < r \leq 2$ are excluded in the well-posedness analysis, depending on the particular setting of the problem (see the above mentioned references).

4 Numerical results

4.1 Constant viscosity, $\operatorname{Re}_\varepsilon \geq 0$

With $\alpha^* = 0$ and $G^* = 0$ (or $r = 2$) in (16), the model reverts to that of an incompressible Navier–Stokes fluid. The non-dimensional plane slider flow problem is then described by the three parameters

$$h_2/h_1, \quad \varepsilon \quad \text{and} \quad \operatorname{Re}_\varepsilon$$

and by the pressure drop (the difference of the constants \hat{P}_0 in (13) on Γ_{in} and Γ_{out}). We prescribe $\hat{P}_0 = 0$ on the both boundaries throughout the paper; this represents the ambient pressure, supposedly negligible in comparison to the characteristic pressure P^* . It is for the sake of simplicity that we keep $\hat{P}_0 = 0$ even for $\operatorname{Re}_\varepsilon > 0$, cf. [10].

The resulting flow has a rather simple structure, as illustrated in Fig. 2 for $h_2/h_1 = 2$, $\operatorname{Re}_\varepsilon = 10$ and $\varepsilon = 0.1$. The velocity field is not far from being unidirectional, its horizontal component \hat{u} having a parabolic profile across the film. A pressure peak is generated in the center part of the domain. The pressure differences across the film vanish for small values of ε , as shown in Fig. 2d for $\varepsilon = 0.005$.

The problem has been studied by Szeri and Snyder [41], where the results obtained using the Reynolds lubrication approximation and the numerical results for a quasi two-dimensional thin-film flow model derived in the paper were compared to the finite element solution to the full Navier–Stokes problem. The pressure differences across the film, quantified for convenience of the presentation by

$$d_{\hat{p}} = \frac{\max_{\hat{x} \in (0,1)} |\hat{p}(\hat{x}, \hat{h}) - \hat{p}(\hat{x}, 0)|}{\max_{\hat{x} \in (0,1)} \hat{p}(\hat{x}, \hat{h})},$$

were computed for the Navier–Stokes solutions, for a reasonable range of parameters, $\operatorname{Re}_\varepsilon$ up to 100 and ε from 0.005

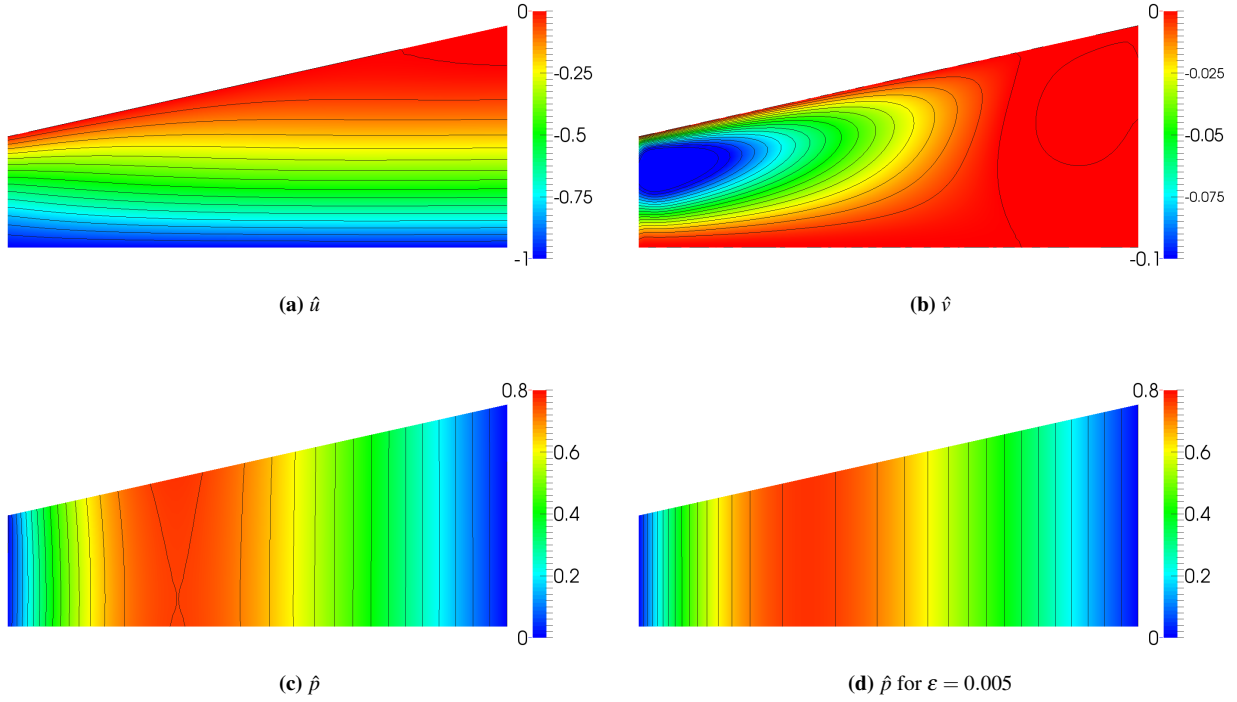


Figure 2: Flow in a slider bearing ($h_2/h_1 = 2$, $\text{Re}_\varepsilon = 10$, (a,b,c) $\varepsilon = 0.1$, (d) $\varepsilon = 0.005$)

h_2/h_1	$\varepsilon = 0.1$	$\varepsilon = 0.01$	$\varepsilon = 0.001$
11.0	1.603	1.580	1.579
3.00	0.5965	0.5917	0.5917
2.25	0.4257	0.4229	0.4228
2.00	0.3597	0.3575	0.3575
1.50	0.2060	0.2050	0.2049
1.20	0.09181	0.09137	0.09136
1.10	0.04791	0.04769	0.04768
1.01	0.004999	0.004975	0.004975

Table 1: Dimensionless lift \hat{F}_y , for different h_2/h_1 and ε ($\hat{\eta} \equiv 1$, $\text{Re}_\varepsilon = 0$)

up to 1. It was observed that $d_{\hat{p}}$ does not increase with Re_ε and that it remains small even for ε rather large. Similarly, the dimensionless pressure peak, $\max_{\hat{\mathbf{x}} \in \hat{\Omega}} \hat{p}(\hat{\mathbf{x}})$, same as the dimensionless force (lift) \hat{F}_y , where⁶

$$\hat{\mathbf{F}} = \begin{pmatrix} \hat{F}_x \\ \hat{F}_y \end{pmatrix} = \int_{\hat{\Gamma}_{\text{slider}}} -\tilde{\mathbf{T}} \hat{\mathbf{n}} d\hat{s}, \quad \text{where } \mathbf{F} = P^* X^* \begin{pmatrix} \varepsilon \hat{F}_x \\ \hat{F}_y \end{pmatrix},$$

was shown to vary strongly with Re_ε and not with ε . Our numerical experiments confirm these conclusions, see Fig. 3a and 4. We, however, observe much smaller values of the pressure differences $d_{\hat{p}}$ than those reported in [41], as compared in Fig. 3b. The explanation for the discrepancy is not clear,

⁶ Note that $d\hat{s} = X^* \sqrt{\hat{n}_y^2 + \varepsilon^2 \hat{n}_x^2} d\hat{s}$.

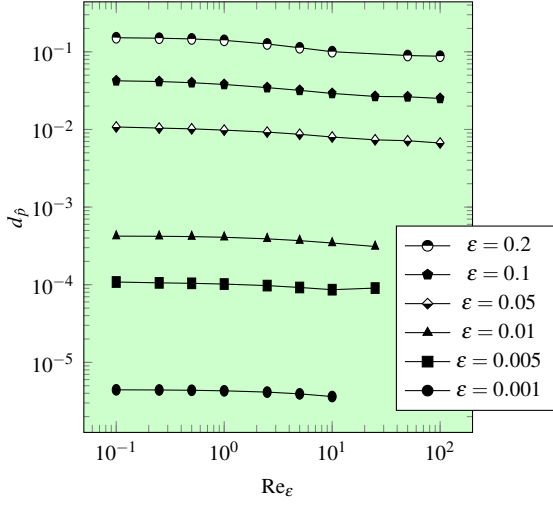
as a detailed discussion of the Navier–Stokes problem formulation and results is lacking⁷ in [41]. Both the computed traction along the slider surface presented in Fig. 4 and the resulting lift for various slopes h_2/h_1 presented in Table 1 show surprisingly small variation with ε . It is worth noting that the values of \hat{F}_y for $\varepsilon = 0.001$ in Table 1 coincide within the presented accuracy with the results obtained from the Reynolds equation, cf. Table 1 in [41], while they provide a surprisingly good approximation even to the problems with $\varepsilon = 0.1$.

4.2 Pressure-thickening, $\alpha^* > 0$. Inappropriateness of the viscosity cut-off procedure and computational difficulties

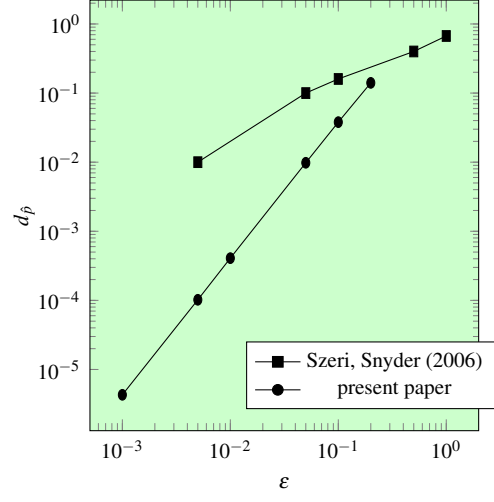
In all the remaining examples, we take $h_2/h_1 = 2$. When $\alpha^* > 0$, the fluid is pressure-thickening. For clarity of exposition, we start with $G^* = 0$, reducing (16) to the exponential pressure–viscosity model $\hat{\eta} = e^{\alpha^* \hat{p}}$. As α^* increases, the other parameters being fixed, the pressure peak generated within the plane slider flow grows; the non-linear character of the system is emphasized and the discrete problem is more difficult to handle. Eventually, for α^* large enough, (19) is violated, bringing about a failure of the numerical scheme. This observation seems in accordance with what has been encountered by other researchers, cf. [1, 26].

In order to prevent the failure of the numerical calculation,

⁷We suspect that boundary conditions different from (5), (13) could have been set on Γ_{in} and Γ_{out} in [41], which might have caused cross flow and pressure gradients in the vicinity of both the artificial boundaries.

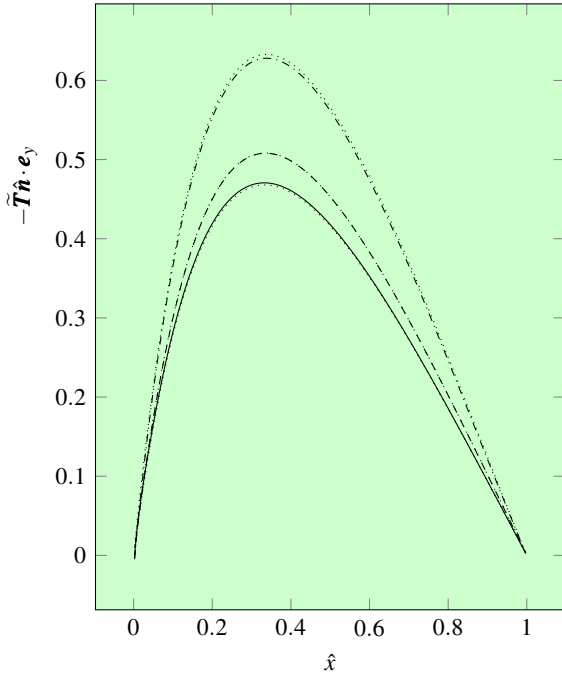


(a) $d_{\hat{p}}$ for various values of ϵ and Re_{ϵ}

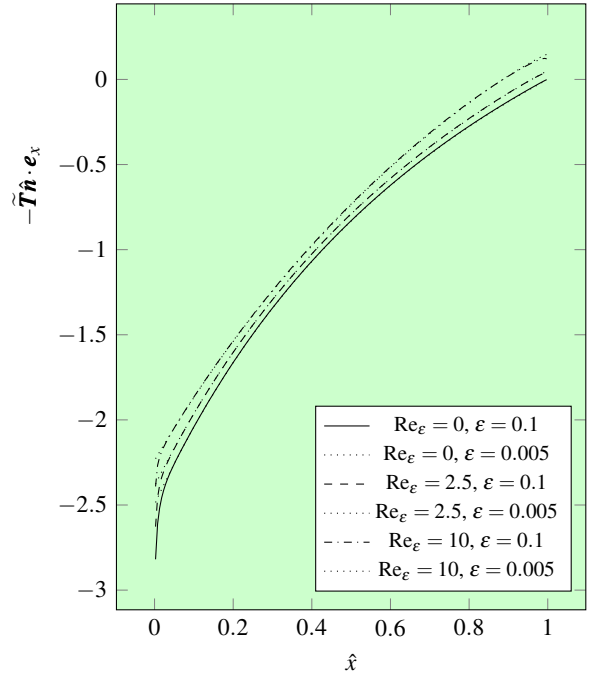


(b) $d_{\hat{p}}$ variation with ϵ , comparison to [41]

Figure 3: Dimensionless pressure difference coefficient $d_{\hat{p}}$ ($h_2/h_1 = 2$ and $\hat{\eta} \equiv 1$)



(a) vertical component, $-\tilde{\mathbf{T}}\hat{\mathbf{n}} \cdot \mathbf{e}_y$



(b) horizontal component, $-\tilde{\mathbf{T}}\hat{\mathbf{n}} \cdot \mathbf{e}_x$

Figure 4: Dimensionless traction vector $-\tilde{\mathbf{T}}\hat{\mathbf{n}}$ along the slider surface $\hat{\Gamma}_{\text{slider}}$ ($h_2/h_1 = 2$ and $\hat{\eta} \equiv 1$)

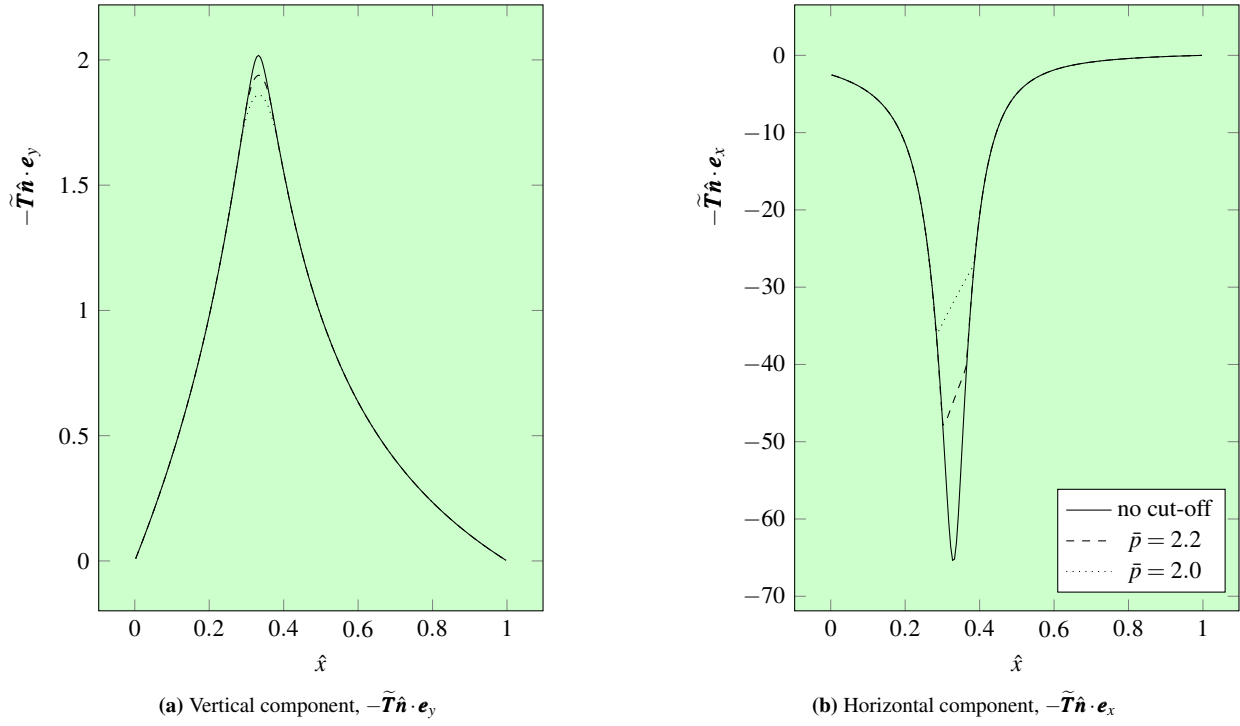


Figure 5: Dimensionless traction along $\hat{\Gamma}_{\text{slider}}$, for $\alpha^* = 1.74$ and different cut-off parameters ($G^* = 0$, $\varepsilon = 0.005$, $\text{Re}_\varepsilon = 0$)

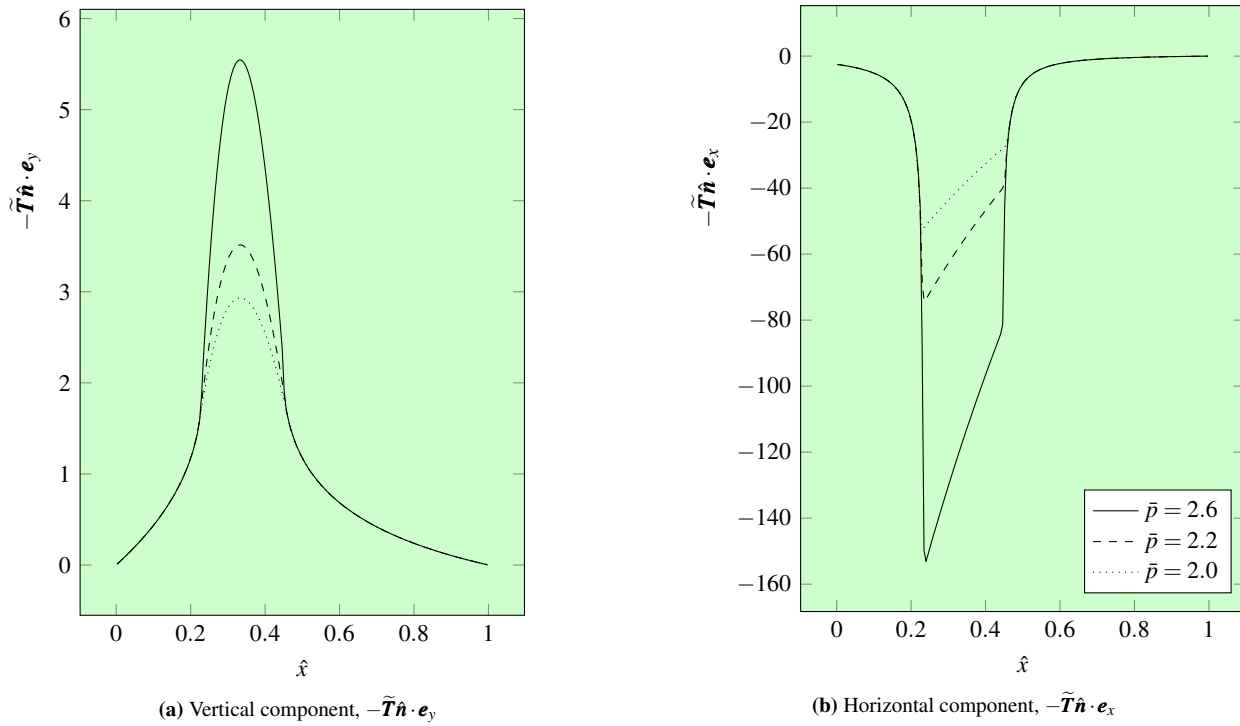


Figure 6: Dimensionless traction along $\hat{\Gamma}_{\text{slider}}$, for $\alpha^* = 1.85$ and three cut-off parameters (no solution without cut-off available)

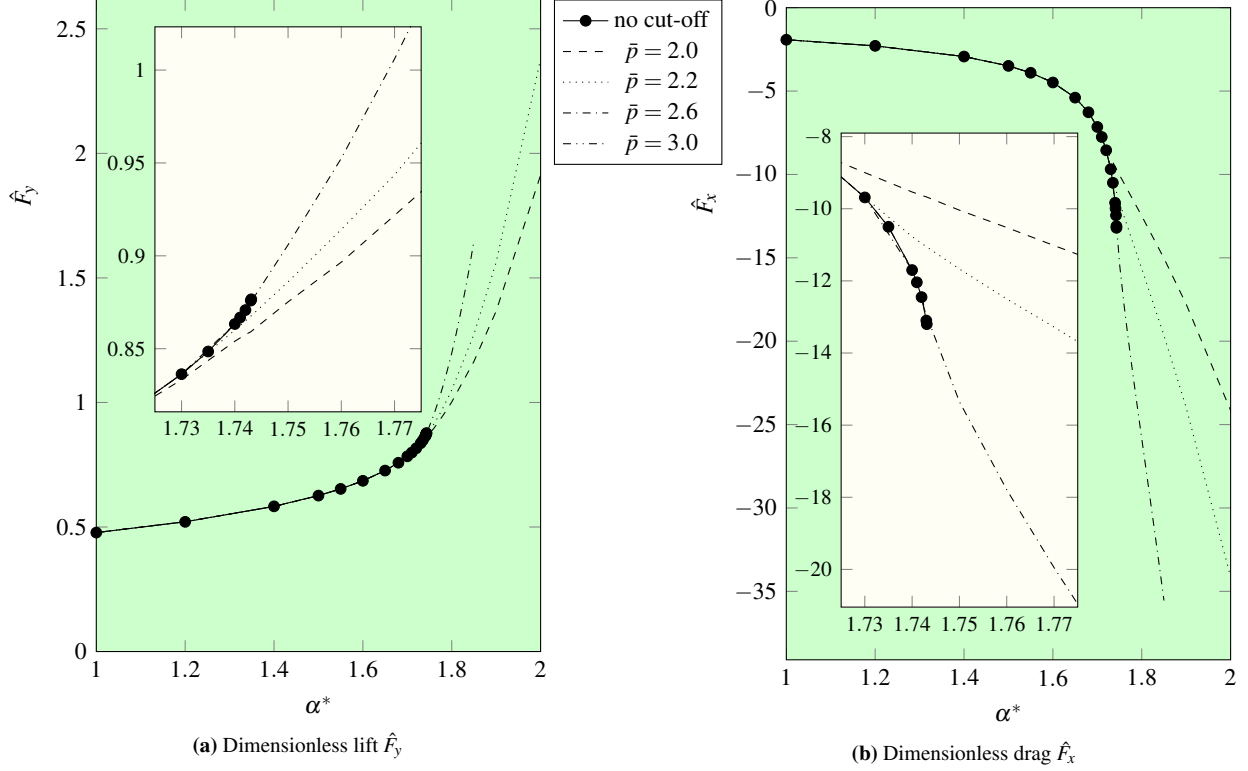


Figure 7: Dimensionless force acting on the slider, for different cut-off parameters ($\text{Re}_\varepsilon = 0$, $G^* = 0$, $h_2/h_1 = 2$, $\varepsilon = 0.005$)

a technique practiced by some researchers has been to cut off the viscosity by employing, e.g.,

$$(20) \quad \hat{\eta}_{\bar{p}} = \hat{\eta}(\min\{\hat{p}, \bar{p}\}, \text{tr}\hat{\mathbf{D}}^2)$$

instead of $\hat{\eta}$, or similarly by imposing a restriction on the norm of stress by employing, e.g.,

$$\hat{\eta}_{\bar{S}} = \min\{\hat{\eta}(\cdot, \cdot) \text{tr}\hat{\mathbf{D}}^2, \bar{S}\} / \text{tr}\hat{\mathbf{D}}^2.$$

To pick some examples wherein such a cut off has been appealed to, we refer to [1, 14, 19, 26, 30]. Doing so, one can ensure $\partial\mathcal{S}/\partial p$ to remain bounded and, by choosing suitable threshold parameter \bar{p} or \bar{S} , to keep (19) fulfilled at least for bounded shear rates. In particular, using (20) and considering for instance (16) and given \bar{D} and C , one can find \bar{p} such that (19) holds for any $\text{tr}\hat{\mathbf{D}}^2 \leq \bar{D}$. One should notice, however, examining (16) with any $\alpha^* > 0$ and G^* , $\beta^* \geq 0$, that for any choice of \bar{p} , (19) is still violated for sufficiently large shear rates.

Surprisingly, the possible sensitivity of the solution and of the derived quantities of interest on the cut-off parameter has not been investigated in the literature so far, to the best of our knowledge. We provide the following set of numerical experiments to document that, once the cut-off takes effect, the results depend solely on the parameter \bar{p} .

For convenience, the comparison is presented for $\varepsilon = 0.005$ and $\text{Re}_\varepsilon = 0$, but we observed that the behaviour is qualitatively the same for higher values of these parameters

as well. The dimensionless traction along the slider surface is presented in Fig. 5, where the results for the unaltered viscosity and for two different cut-off parameters are compared for $\alpha^* = 1.74$. Note that while the vertical component (which corresponds almost exactly to the pressure distribution and sums up to the resulting lift force) does not vary considerably in this example, the horizontal component (which determines the resulting friction) is affected substantially. The differences are even more pronounced in Fig. 6. For $\alpha^* = 1.85$, we were unable to find any solution with unaltered viscosity, the condition (19) being eventually violated while attempting to solve the discrete nonlinear system. Therefore we only present the results for three values of \bar{p} , showing a marked variation in both components of the traction.

In terms of the resulting force as a function of α^* , the comparison is presented in Fig. 7. For $\alpha^* < 1.72$, the maximum of the resulting dimensionless pressure does not reach the lowest cut-off threshold $\bar{p} = 2.0$, hence all the curves plotted in Fig. 7 coincide up to that value. With the unaltered model, we were only able to proceed up to $\alpha^* = 1.743$, same as in the case with $\bar{p} = 3.0$. With $\bar{p} = 2.6$, the computation fails for $\alpha^* \geq 1.86$. Fig. 7 illustrates that once the viscosity cut-off takes effect, the resulting force is altered significantly. We may conclude, that while the lower cut-off parameters may seem to add to the robustness of the computation, they actually entail strikingly different results depending on the choice of \bar{p} , making such solutions unreliable.

To enhance the illustration, we present the comparison of

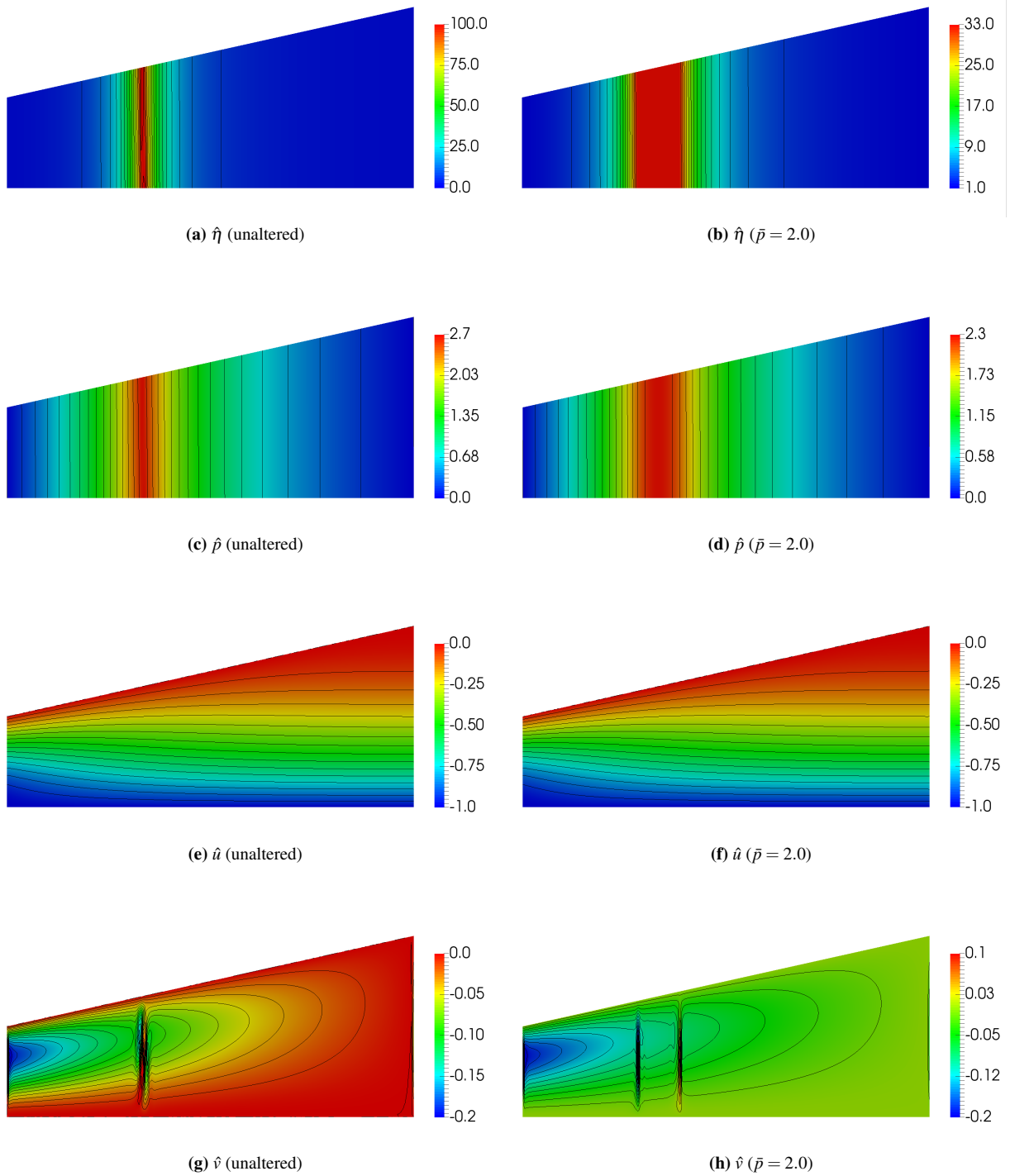


Figure 8: Dimensionless viscosity $\hat{\eta}$, pressure \hat{p} and velocity $\hat{\mathbf{u}}$ for $\alpha^* = 1.743$, for unaltered viscosity (left) and using the cut off (right), ($G^* = 0.0$, $\varepsilon = 0.005$, $\text{Re}_\varepsilon = 0$)

the solutions with unaltered viscosity and with the cut-off defined by $\bar{p} = 2.0$ in Fig. 8, for the case $\alpha^* = 1.743$. The dimensionless pressure peak in the unaltered case reaches $\hat{p} = 2.7$ (c), while with the cut viscosity it is lowered to $\hat{p} = 2.3$ (d). The difference is more pronounced in the cor-

responding maximal values of the viscosity, the peak value $\hat{\eta} = 100$ (a) is lowered to $\hat{\eta} = 33$ (b), the viscosity now being constant in a substantial part of the domain around the pressure peak. Moreover, while the differences in the horizontal component \hat{u} of the dimensionless velocity can not be

distinguished visually (e,f), there is a striking difference in its vertical component \hat{v} . While the unaltered case (g) results in a distinct rib in \hat{v} , related to the non-negligible variation of the viscosity with pressure in the vicinity of the pressure and viscosity peak, in the altered case (h) the rib is replaced by two stronger artefacts positioned where the artificial viscosity cut off takes effect.

In all what follows, we use the unaltered viscosity (16).

4.3 Pressure variations across the film induced by pressure-thickening

Within a unidirectional flow, such as Couette flow or plane Poiseuille flow, of a Navier–Stokes fluid or a fluid with shear rate dependent viscosity, in the absence of body forces, the pressure gradient is either trivial or its direction is that of the flow. In the context of lubrication flows, the almost unidirectional flow within the thin film then corresponds to negligible pressure variations across the film. The situation differs significantly if the viscosity varies with the pressure. This was well documented for the Couette and Poiseuille plane flows, see e.g. [6, 23, 24]. In fact, for the exponential pressure–viscosity relation $\eta = e^{\alpha p}$ no such unidirectional flow can be found (except, interestingly enough, the case with a cross-flow pressure gradient due to the gravitational force, see [32]). It was pointed out in [36] that the cross-flow pressure gradient induced within the lubrication flow in the piezoviscous regime gives rise to an additional term in the Reynolds approximation equation, see also [7, 18].

The results of numerical computations presented in Fig. 9 reveal how the pressure differences appear with increasing α^* , for different values of ε . Notice again that each plotted curve ends at certain critical value of α^* , for which (and all the higher values) the condition (19) is violated and the numerical scheme fails. An increase in the coefficient $d_{\bar{p}}$ by as much as two orders of magnitude, when compared to the Navier–Stokes fluid at given ε , can be observed before such critical α^* is reached. Simultaneously, a rapid increase of the maximal dimensionless pressure (not visualised) and both components of the resulting force $\hat{\mathbf{F}}$ appear. Note how the critical values of α^* differ with ε , say for $\varepsilon > 0.01$, as can be read from Fig. 9. We observe that for $\alpha^* > 0$ the resulting dimensionless force is more sensitive to ε than it was shown for a Navier–Stokes lubricant, cf. Fig. 4.

4.4 The shear-thinning and inertial effects

We complete the presentation of the numerical computations by including a sample of results with shear-thinning, i.e. with $G^* > 0$, and the results for $\text{Re}_\varepsilon > 0$, in addition to pressure-thickening. The observed coefficient $d_{\bar{p}}$ and the resulting dimensionless force are again plotted in Figs. 10 and 11. For the simplicity of presentation we keep $r = 3/2$ and $\beta/\alpha = 2$ and only present the results for $\varepsilon = 0.005$.

For $\alpha^* > 0$ and small values of ε , the numerical simulations for positive Re_ε are more demanding in comparison to the case $\alpha^* = 0$. In contrast to the results presented in

Fig. 3a, we observed that the discrete solutions for, let us say, $\alpha^* > 1.5$ with $\text{Re}_\varepsilon = 5$ or higher remain mesh-dependent for regular mesh refinements as fine as $\hat{h} \sim 2^{-6}$ (corresponding to 136194 degrees of freedom). The comparison of the resulting $d_{\bar{p}}$ and $\hat{\mathbf{F}}$ for $\text{Re}_\varepsilon = 0$ and 2.5 is plotted in Fig. 10, illustrating how the increased modified Reynolds number leads (by means of increasing the generated pressure peak) to the increased dimensionless force. The approximation obtained for $\text{Re}_\varepsilon = 5$ is included as the dotted line. Further study of the *combined* effects of pressure-thickening and higher Reynolds numbers would require some additional care which we exclude from the current presentation.

With the shear-thinning taking effect, the growth of the maximal pressure and viscosity with increasing α^* is postponed, thus increasing significantly the observed critical value of α^* for which (19) is violated within the resulting flow. More detailed comparison is provided in Fig. 12, where the distribution of the dimensionless traction along the slider surface is plotted for five combinations of α^* and G^* . All these results are for $\text{Re}_\varepsilon = 0$ and $\varepsilon = 0.005$.

For reference, the solid line is plotted in Fig. 12 representing a constant viscosity lubricant. The dashed line then shows the pure piezoviscous regime with $\alpha^* = 1.7$, displaying the large sharp pressure peak on the left plot and the increased friction contributions due to the corresponding peak in the viscosity, on the right-hand side plot. With the same α^* but with $G^* = 0.5$, as can be read from the dotted line, the effect of piezoviscous response is largely counteracted by shear-thinning. For comparison, the case of $G^* = 0.5$ but $\alpha^* = 0$ is also included, showing much lesser variation due to shear-thinning in the case of $\alpha^* = 0$, when compared to the piezoviscous regime for $\alpha^* = 1.7$.

Finally, we include the dashed-double-dotted plot for the case $\alpha^* = 4.4$ and $G^* = 0.5$, to emphasize the difference in influence of these two parameters on the two components of the resulting force: Note that for $\alpha^* = 4.4$, $G^* = 0.5$ the vertical traction (and so the pressure peak) almost reaches the values for the pure piezoviscous $\alpha^* = 1.7$, $G^* = 0.0$, the peak being slightly sharper and shifted towards the inlet. By contrast, significantly larger horizontal traction is observed.

The distribution of the dimensionless viscosity in $\hat{\Omega}$ is presented by means of contour plots in Fig. 13, for the same four cases: (a) the pure piezoviscous case $\alpha^* = 1.7$, $G^* = 0$, showing a sharp viscosity peak reaching the maximum $\hat{\eta} = 24$, (b) the case $\alpha^* = 1.7$, $G^* = 0.5$, where the viscosity peak is an order of magnitude lower (which is also accompanied by the significantly lower pressure peak), (c) the pure shear-thinning case $\alpha^* = 0$, $G^* = 0.5$, and finally (d) the case $\alpha^* = 4.4$, $G^* = 0.5$, showing the viscosity peak reaching the maximum $\hat{\eta} = 60$ as well as the variation of the viscosity due to the velocity gradient in the remaining parts of the domain.

5 Conclusion

Based on the numerical computations that have been carried out, we conclude that the finite element solution for the pla-

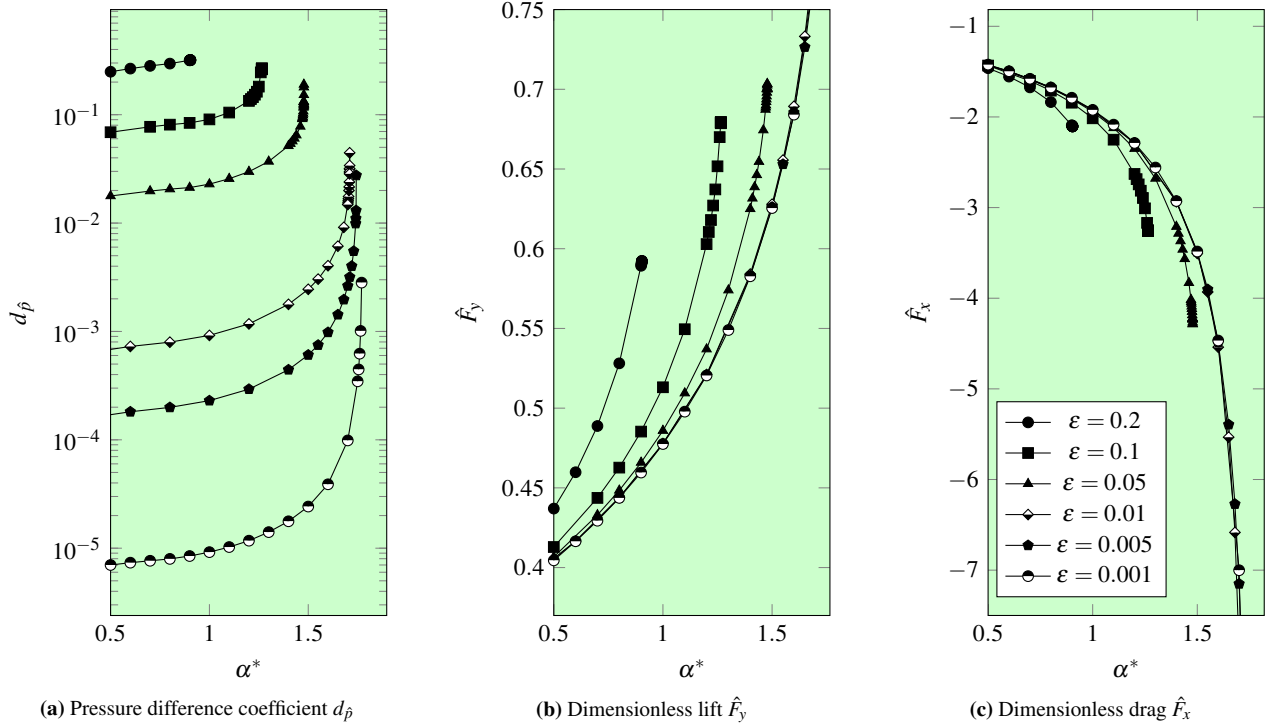


Figure 9: Dimensionless force \hat{F} and pressure difference coefficient $d_{\hat{p}}$, variation with ϵ and α^* ($h_2/h_1 = 2, Re_\epsilon = 0, G^* = 0$)

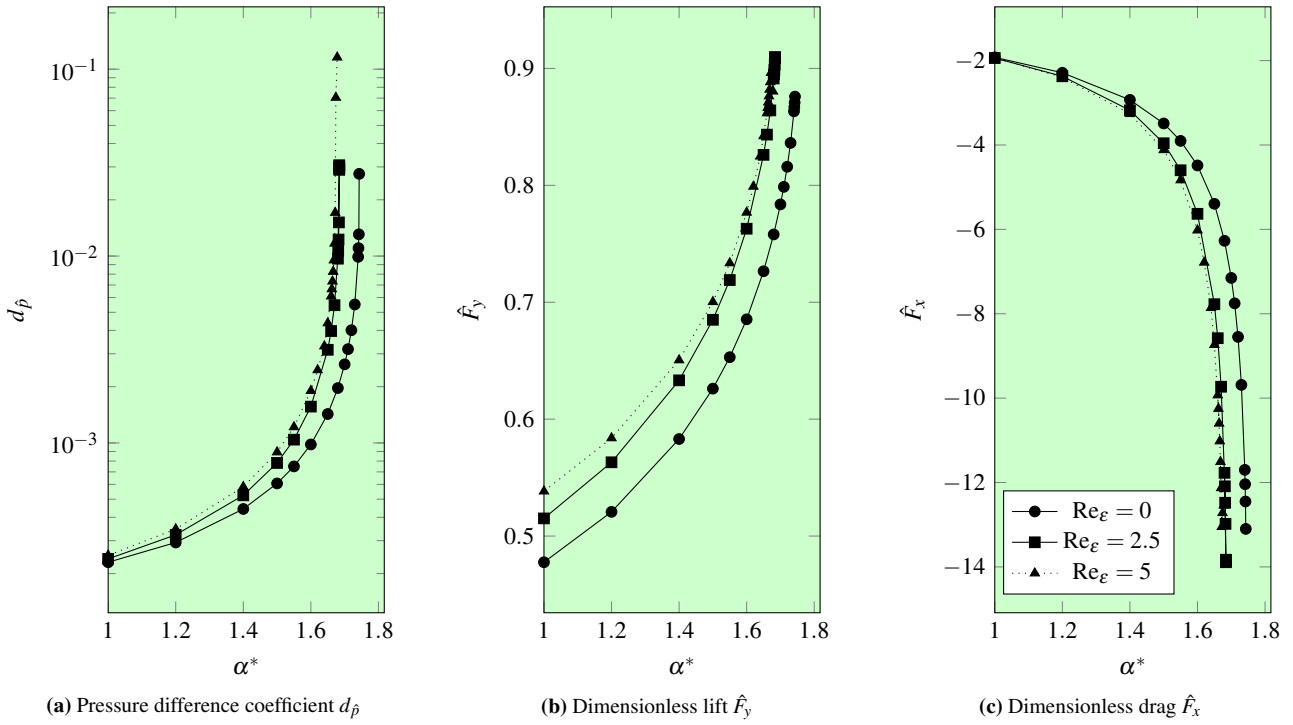


Figure 10: Dimensionless force \hat{F} and pressure difference coefficient $d_{\hat{p}}$, for various Re_ϵ and α^* ($h_2/h_1 = 2, G^* = 0, \epsilon = 0.005$)

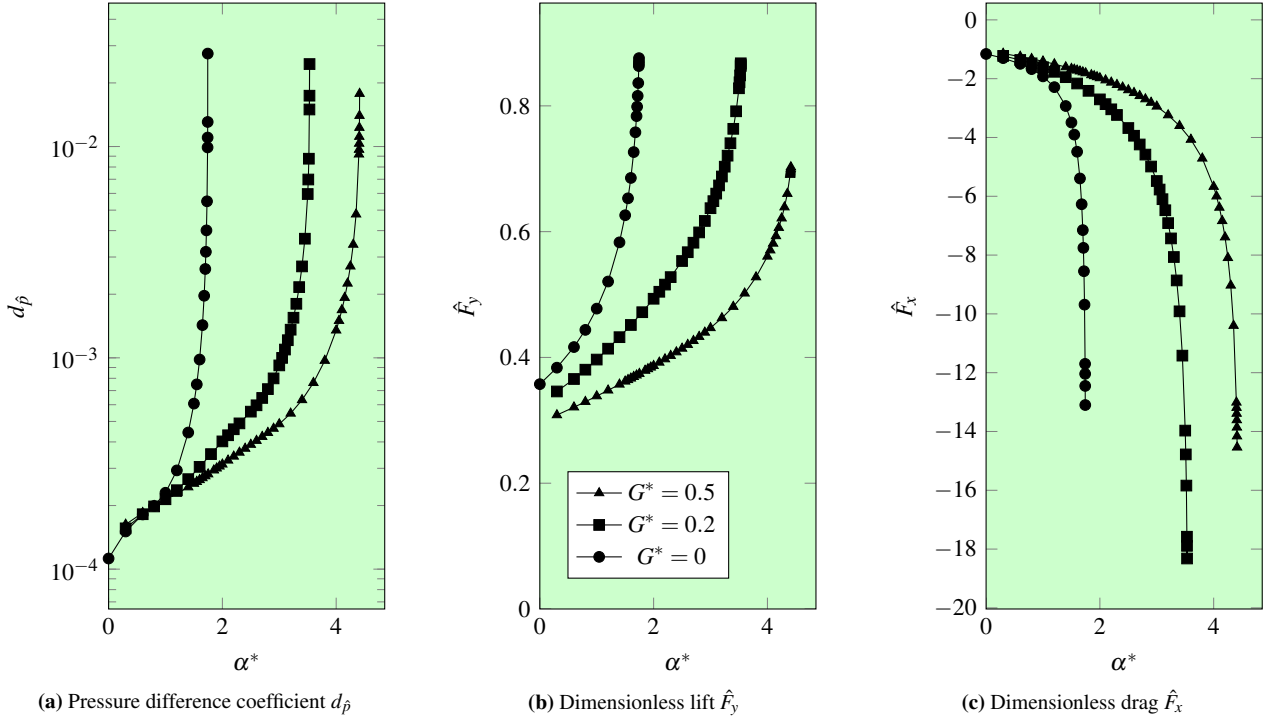


Figure 11: Dimensionless force $\hat{\mathbf{F}}$ and pressure difference coefficient $d_{\hat{p}}$, variation with G^* and α^* ($h_2/h_1 = 2$, $\text{Re}_\varepsilon = 0$, $\varepsilon = 0.005$ and $r = 3/2$, $\beta/\alpha = 2$)

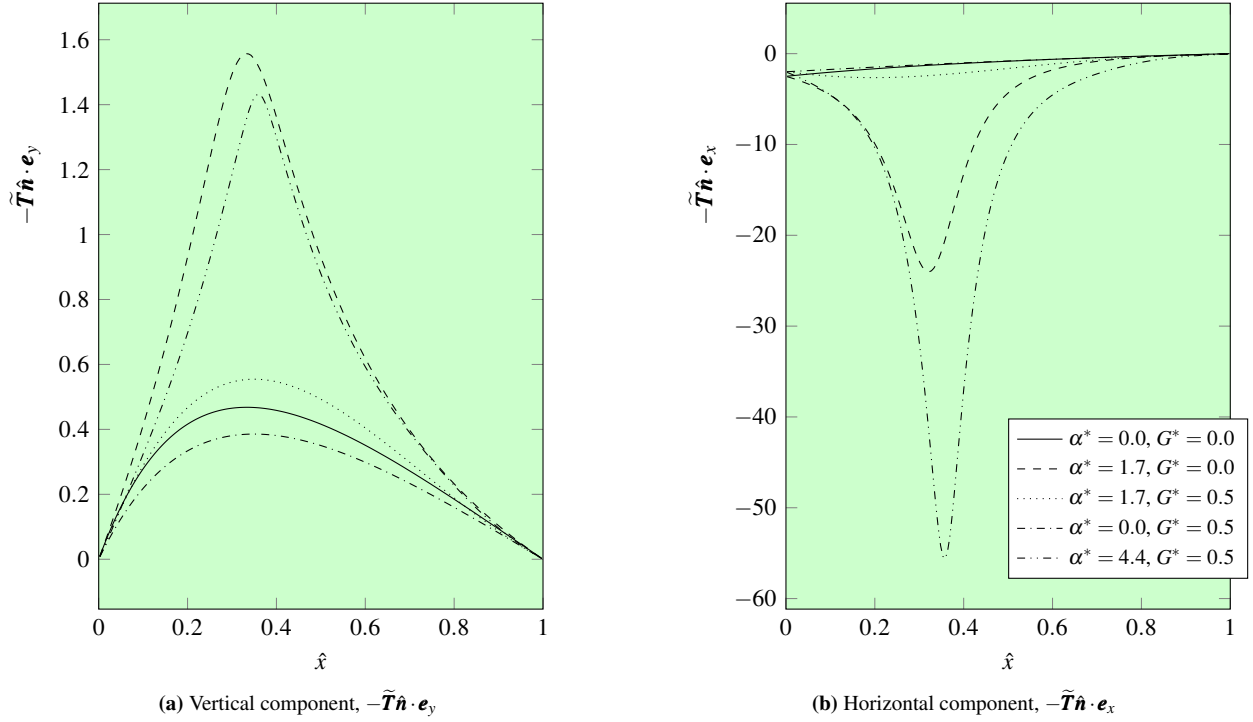


Figure 12: Traction along the slider surface $\hat{\Gamma}_{\text{slider}}$ for selected α^* and G^* ($h_2/h_1 = 2$, $\text{Re}_\varepsilon = 0$, $\varepsilon = 0.005$, and $r = 3/2$, $\beta/\alpha = 2$)

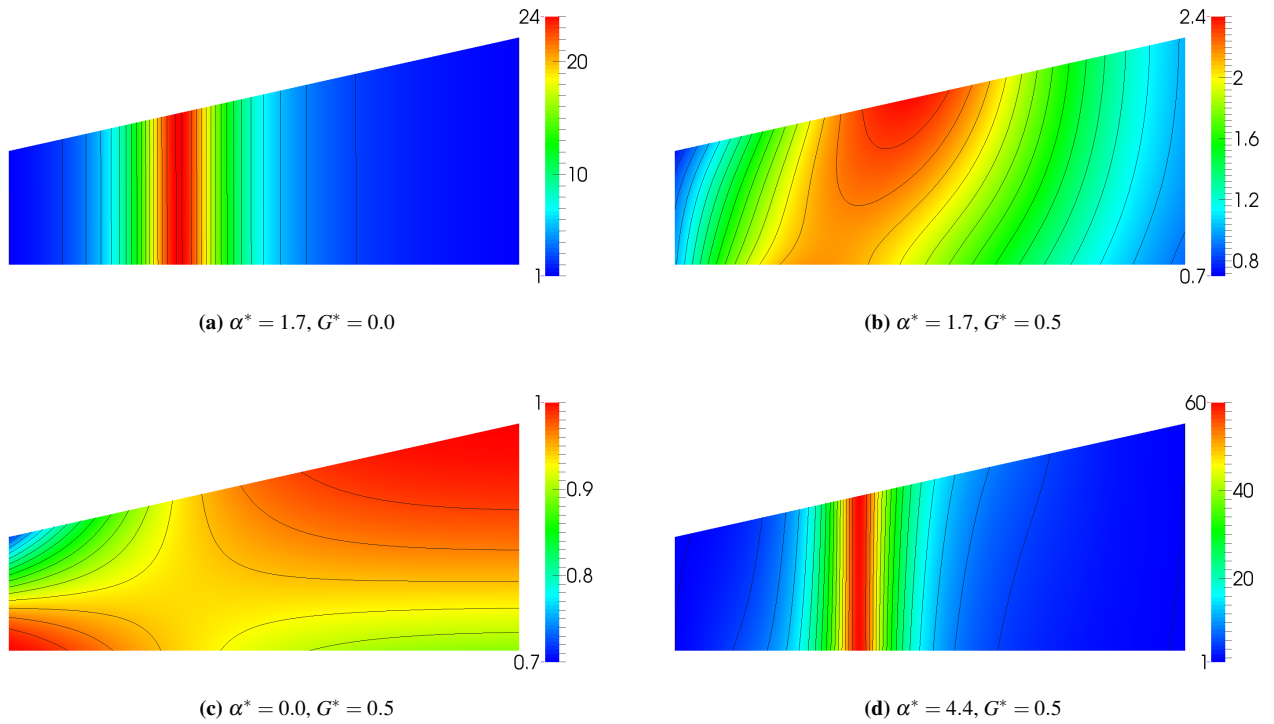


Figure 13: Dimensionless viscosity $\hat{\eta}$ for selected α^* and G^* (h_2/h_1 , $\text{Re}_\varepsilon = 0$, $\varepsilon = 0.005$, and $r = 3/2$, $\beta/\alpha = 2$)

near steady isothermal flow of an incompressible fluid with pressure and shear rate dependent viscosity can be obtained as long as the condition (19) is satisfied. Note that the condition (19) supplemented by certain additional assumptions also guarantees the existence of solutions to the full equations governing the flows of the fluids under consideration. Once the condition is violated, i.e. if the pressure *or* shear rate reach values larger than some critical value, we were unable to obtain any numerical solution.

As the parameters approach the critical case, the rapid growth of the quantities tracked in the plane slider simulations, such as the maximal values of the pressure and viscosity and the force acted on the solid surfaces, were observed.

In particular, we have documented the implications of cutting the viscosity off above a given threshold of pressure: the technique does not guarantee convergence and, once the cut-off takes effect, the results depend critically on the artificial threshold parameter. The effect is particularly pronounced when the overall friction (i.e. the tangential part of the traction observed on the solid walls) is considered.

In the range of parameters where the unaltered viscosity can be considered, we discussed the resulting plane slider flow for a number of combinations of the dimensionless parameters related to the pressure-thickening, shear-thinning, inertia and geometry. In particular, we tracked the force acting on the slider surface as it varies with the dimensionless pressure–viscosity coefficient α^* for different parameters ε , where $\varepsilon \searrow 0$ would represent the lubrication approximation limit, and with different parameters G^* related to the activa-

tion of the shear-thinning response.

In order to study the variations of pressure and other quantities across the film, the boundary conditions taken on the artificial (inflow and outflow) boundaries needed to be discussed. We have observed that the condition (5), derived in Sect. 2.3 based on the *do-nothing* condition used for Navier–Stokes fluid, is appropriate for the problem under consideration. In contrast to, e.g., constant traction being prescribed, we observed smooth solutions without any artifacts in the pressure or viscosity field in the vicinity of the artificial boundaries.

We have displayed how the pressure variations across the film appear within the flow due to pressure-thickening. The results may imply that the lubrication assumptions are violated by the piezoviscous lubricant. This assertion has been made already by researchers working with the Reynolds approximation, and it was our hope to provide a numerical validation to the recently derived corrections of Reynolds equation. Unfortunately, as the appearance of pressure variations is in conjunction with the change of the structure in the momentum equation, the most important comparison would require one to find a numerical solution to the problem in the case, where the condition (19) is violated. This represents a challenging open problem in computational fluid dynamics of incompressible fluids. To the best of our knowledge, no numerical solutions have been reported in the literature so far that would reach beyond (19). Similarly, there are no theoretical results either, concerning the existence of such a solution.

References

- [1] Almqvist T, Larsson R (2002) The Navier-Stokes approach for thermal EHL line contact solutions. *Tribol Int* 35(3):163–170, DOI 10.1016/S0301-679X(01)00112-8
- [2] Almqvist T, Larsson R (2008) Thermal transient rough EHL line contact simulations by aid of computational fluid dynamics. *Tribol Int* 41(8):683–693, DOI 10.1016/j.triboint.2007.11.004
- [3] Almqvist T, Almqvist A, Larsson R (2004) A comparison between computational fluid dynamic and Reynolds approaches for simulating transient EHL line contacts. *Tribol Int* 37(1):61–69, DOI 10.1016/S0301-679X(03)00131-2
- [4] Bair S (2006) Reference liquids for quantitative elastohydrodynamics: selection and rheological characterization. *Tribol Lett* 22(2):197–206, DOI 10.1007/s11249-006-9083-y
- [5] Bair S (2007) High Pressure Rheology for Quantitative Elastohydrodynamics. *Tribol. Interface Eng.*, Elsevier Science
- [6] Bair S, Khonsari M, Winer WO (1998) High-pressure rheology of lubricants and limitations of the Reynolds equation. *Tribol Int* 31(10):573–586
- [7] Bayada G, Cid B, García G, Vázquez C (2013) A new more consistent Reynolds model for piezoviscous hydrodynamic lubrication problems in line contact devices. *Appl Math Modell* 37(18-19):8505–8517, DOI 10.1016/j.apm.2013.03.072
- [8] Bruneau CH, Fabrie P (1996) New efficient boundary conditions for incompressible Navier-Stokes equations: A well-posedness result. *RAIRO—Math Modell Numer Anal* 30(7):815–840
- [9] Bruyere V, Fillot N, Morales-Espejel GE, Vergne P (2012) Computational fluid dynamics and full elasticity model for sliding line thermal elastohydrodynamic contacts. *Tribol Int* 46(1):3–13, DOI 10.1016/j.triboint.2011.04.013
- [10] Buckholz RA (1987) The effect of lubricant inertia near the leading edge of a plane slider bearing. *J Tribol* 109(1):60–64, DOI 10.1115/1.3261328
- [11] Bulíček M, Málek J, Rajagopal KR (2009) Analysis of the flows of incompressible fluids with pressure dependent viscosity fulfilling $\nu(p, \cdot) \rightarrow +\infty$ as $p \rightarrow +\infty$. *Czechoslovak Math J* 59(2):503–528
- [12] Bulíček M, Málek J, Rajagopal KR (2009) Mathematical analysis of unsteady flows of fluids with pressure, shear-rate and temperature dependent material moduli that slip at solid boundaries. *SIAM J Math Anal* 41(2):665–707
- [13] Bulíček M, Majdoub M, Málek J (2010) Unsteady flows of fluids with pressure dependent viscosity in unbounded domains. *Nonlin Anal: Real World Appl* 11(5):3968–3983, DOI 10.1016/j.nonrwa.2010.03.004
- [14] Davies AR, Li XK (1994) Numerical modelling of pressure and temperature effects in viscoelastic flow between eccentrically rotating cylinders. *J Non-Newton Fluid Mech* 54:331–350
- [15] Davies TA (2004) UMFPAK version 4.3 user guide. Tech Rep REP-2004-349, University of Florida (<http://www.cise.ufl.edu/research/sparse/umfpack>)
- [16] Franta M, Málek J, Rajagopal KR (2005) On steady flows of fluids with pressure- and shear-dependent viscosities. *Proc R Soc Lond A* 461(2055):651–670, DOI 10.1098/rspa.2004.1360
- [17] Gresho PM, Sani RL (2000) Incompressible flow and the finite element method., vol 2: Isothermal laminar flow. John Wiley & Sons Ltd
- [18] Gustafsson T, Rajagopal KR, Stenberg R, Videman J (2015) Nonlinear Reynolds equation for hydrodynamic lubrication. *Appl Math Modell* 39(17):5299–5309, DOI 10.1016/j.apm.2015.03.028
- [19] Gwynllwy DR, Davies AR, Phillips TN (1996) On the effects of piezoviscous lubricant on the dynamics of a journal bearing. *J Rheol* 40:1239–1266
- [20] Hartinger M, Dumont ML, Ioannides S, Gosman D, Spikes H (2008) CFD Modeling of a Thermal and Shear-Thinning Elastohydrodynamic Line Contact. *J Tribol* 130(4):041,503, DOI 10.1115/1.2958077
- [21] Heywood JG, Rannacher R, Turek S (1996) Artificial boundaries and flux and pressure conditions for the incompressible Navier–Stokes equations. *Int J Numer Meth Fluids* 22(5):325–352
- [22] Hirn A, Lanzendörfer M, Stebel J (2012) Finite element approximation of flow of fluids with shear-rate- and pressure-dependent viscosity. *IMA J Numer Anal* 32(4):1604–1634, DOI 10.1093/imanum/drr033
- [23] Hron J, Málek J, Rajagopal KR (2001) Simple flows of fluids with pressure-dependent viscosities. *Proc R Soc Lond A* 457(2011):1603–1622
- [24] Hron J, Málek J, Průša V, Rajagopal KR (2011) Further remarks on simple flows of fluids with pressure-dependent viscosities. *Nonlin Anal: Real World Appl* 12(1):394–402
- [25] Janečka A, Průša V (2014) The motion of a piezoviscous fluid under a surface load. *Int J Non-Lin Mech* 60:23–32, DOI 10.1016/j.ijnonlinmec.2013.12.006
- [26] Knauf S, Frei S, Richter T, Rannacher R (2013) Towards a complete numerical description of lubricant film dynamics in ball bearings. *Comput Mech* 53(2):239–255, DOI 10.1007/s00466-013-0904-1
- [27] Kračmar S, Neustupa J (2001) A weak solvability of a steady variational inequality of the Navier–Stokes type with mixed boundary conditions. *Nonlin Anal: Theory, Methods & Appl* 47(6, Part 6 Sp. Iss. SI):4169–4180, DOI 10.1016/S0362-546X(01)00534-X
- [28] Lanzendörfer M (2009) On steady inner flows of an incompressible fluid with the viscosity depending on the pressure and the shear rate. *Nonlin Anal: Real World Appl* 10(4):1943–1954, DOI 10.1016/j.nonrwa.2008.02.034

- [29] Lanzendörfer M, Stebel J (2011) On pressure boundary conditions for steady flows of incompressible fluids with pressure and shear rate dependent viscosities. *Appl Math* 56(3):265–285, DOI 10.1007/s10492-011-0016-1
- [30] Li XK, Davies AR, Phillips TN (2000) A transient thermal analysis for dynamically loaded bearings. *Computers and Fluids* 29(7):749–790, DOI 10.1016/S0045-7930(99)00035-3
- [31] Lugt PM, Morales-Espejel GE (2011) A review of elastohydrodynamic lubrication theory. *Tribol Trans* 54(3):470–496, DOI 10.1080/10402004.2010.551804
- [32] Málek J, Rajagopal KR (2007) Mathematical properties of the solutions to the equations governing the flow of fluids with pressure and shear rate dependent viscosities. In: Friedlander S, Serre D (eds) *Handbook of Mathematical Fluid Dynamics*, vol IV, 1st edn, North Holland, chap 7, pp 407–444
- [33] Neustupa T (2016) A steady flow through a plane cascade of profiles with an arbitrarily large inflow—the mathematical model, existence of a weak solution. *Appl Math Comput* 272, Part 3:687–691, DOI 10.1016/j.amc.2015.05.066
- [34] Průša V, Rajagopal KR (2013) A note on the modeling of incompressible fluids with material moduli dependent on the mean normal stress. *Int J Non-Lin Mech* 52:41–45, DOI 10.1016/j.ijnonlinmec.2013.01.003
- [35] Rajagopal KR (2015) Remarks on the notion of “pressure”. *Int J Non-Lin Mech* 71:165–172, DOI 10.1016/j.ijnonlinmec.2014.11.031
- [36] Rajagopal KR, Szeri AZ (2003) On an inconsistency in the derivation of the equations of elastohydrodynamic lubrication. *Proc R Soc Lond A* 459:2771–2787
- [37] Řehoř M, Průša V (2016) Squeeze flow of a piezoviscous fluid. *Appl Math Comput* 274:414–429, DOI 10.1016/j.amc.2015.11.008
- [38] Reynolds O (1886) On the theory of lubrication and its application to Mr. Beauchamp Tower’s experiments, including an experimental determination of the viscosity of olive oil. *Phil Trans R Soc Lond* 177:157–234
- [39] Sani RL, Gresho PM, Lee RL, Griffiths DF (1981) The cause and cure of the spurious pressures generated by certain FEM solutions of the incompressible Navier–Stokes equations. *Int J Numer Methods Fluids* 1:17–43 (Part I), 171–204 (Part II)
- [40] Szeri AZ (2011) *Fluid Film Lubrication: Theory and Design*, 2nd edn. Cambridge University Press
- [41] Szeri AZ, Snyder V (2006) Convective inertia effects in wall-bounded thin film flows. *Meccanica* 41(5):473–482, DOI 10.1007/s11012-006-0006-7